13-0401

Status of LLRRA-21 and Simulation of Apollo Behavior

D. Currie (1), B. Behr (1), G. Delle Monache (2), S. Dell'Agnello (2)

(1) Department of Physics, University of Maryland, College Park, MD, USA
(2) Istituto Nazionale di Fisica Nucleare Laboratori Nazionali di Frascati, Frascati, Italy
currie@umd.edu

Abstract

The current status of the simulations for the "Lunar Laser Ranging Retroreflector for the 21st Century" [1 Currie], [2 Currie] and the Apollo arrays will be discussed. This paper will address the structure of the latest simulations and the resultant challenges, particularly in the choice of optimal thermal coatings. The simulations of the Apollo arrays will particularly address the role of the dust and the implications of the lunar eclipse observations as they suggest limitations and new directions for the next-generation retroreflector packages.

Background

The retroreflector arrays deployed during the Apollo 11, 14 and 15 missions [3 Alley], [4 Alley], [5 Bender] continue to operate and provide the basis for new and unique science [6 Williams], [7 Williams] [8 Williams], [9 Merkowitz] more than four decades after they were deployed. In addition, the accuracy of the range data obtained from the timing of a single photoelectron return has improved by a factor of more than 200 as the lunar laser ranging stations have implemented various new technologies [10 Murphy]. However, over the past 40 years, the magnitude of the signal (the number of photo-electrons that return for a given amount of transmitted power) has decreased by a factor of ten to one hundred, depending upon the time in the lunar cycle [11 Murphy].
The typical observations of the strength of the returns address the behavior during quasi-equilibrium conditions; that is, the changes in the solar illumination and thus the thermal inputs to the arrays change slowly compared to the thermal time constants of the Cube Corner Reflectors (CCRs) and the housing. However, detailed laser ranging observations were obtained during the lunar eclipse of 21 December 2010 at the APOLLO station. In this case, the changes in the solar illumination and thus the changes in the regolith temperature are similar to the time constants of the CCRs and the housing. This situation allows a much more critical investigation of the optical/thermal properties of the arrays.

On the other hand, there is a very critical balance between the influence of different effects due to coatings, conductivities and geometry. This means that effects that may seem relatively small can throw the balance in one direction or the other. This has led to the necessity of including as many effects as possible in our simulations and analysis.

In preparation for the design, fabrication and deployment of the "Lunar Laser Ranging Retroreflector Array for the 21st Century" (LLRRA-21) [1 Currie], [2 Currie] a detailed set of simulation programs has been developed. This set of programs has then been modified significantly to be able handle the existing Apollo arrays in addition to the planned future arrays. In a later paper, the results of these simulations of the Apollo arrays will be compared to the results of the observations made from the APOLLO ground station.

Structure of Optical/Thermal Lunar Retroreflector Simulation

Philosophy

We shall now address the structure of the simulation. While this can be done in terms of a detailed flow chart (as seen in Figure 14) we first proceed with a more pedagogical approach, that is, a step by step discussion of the individual effects that must be considered and the methods used to address these effects.

Modeling of Solar Input to CCR, the Retaining Ring and the Pocket.

Aspects of a Perfect CCR:

Initially, we will consider a "perfect" CCR that is illuminated by the sun directly overhead. This is the condition that occurs at full moon. In particular, we will consider the effect of various coatings on the back surface and front surface of the CCR. The simulation will address a single CCR in the form of a single "cell" in the panel, which in the case of the Apollo arrays consists of 100 CCRs arranged in a square pattern for Apollo 11 and 14 and 300 CCRs arranged 12 by 25 for Apollo 15.

Metal Coating:

Traditionally CCRs have a metallic coating on the back faces. This leads to a narrow return beam. On the other hand, the metal coating absorbs sunlight. This heat load creates thermal gradients that result in gradients in the index of refraction that induce unacceptable aberrations in the returning laser wave front.

Total Internal Reflection (TIR):

TIR implies that there is no coating (metallic or otherwise) on the back faces of the CCR. This has the advantage that there is no heat load due to the absorption of solar energy on the back faces. This is essential for operating the array during lunar day. On the other hand, there are two disadvantages. The first is that only about 40% of the input laser radiation is concentrated in the central beam. The second issue is that during illumination by the sun at off-axis angles, there is breakthrough of the radiation and all of the solar energy is not reflected by the CCR but some is deposited behind the CCR. This will be addressed later.

Anti-Reflection Coating:

For CCRs deployed on satellites, it is typical to use an anti-reflection coating on the front face. This will increase the return by ~5%. However, there is no information on the survival of such a coating in the harsh environment of the lunar surface. Thus such a coating was not used in order to increase the probability of a decades long life of the proper operation of the retroreflector array.

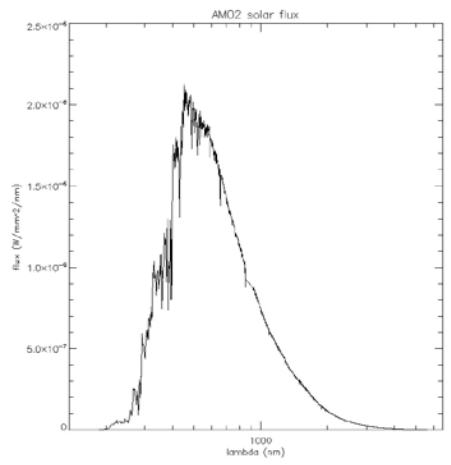

Figure 1 This illustrates the solar spectrum, which is AMO2.

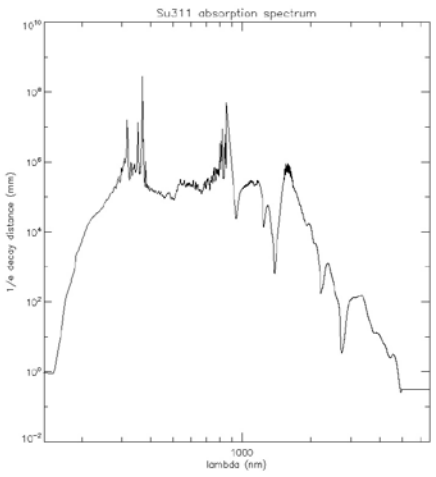

Figure 2 This illustrates the absorption depth for a 1/e loss in the strength of the incoming ray in Heraeus SupraSil 311 Fused silica.

Heat Loads due to Solar Absorption in the CCR

The volumetric absorption of the solar radiation is rather complicated. Each wavelength has a different rate of absorption and thus heat loads deposited at various points in the CCR are quite different. For this initial discussion, we will consider the sun directly over the CCR, that is, during full moon. Since there does not appear to be a commercial program that handles the volumetric absorption, we have developed such a program based on the IDL [12 IDL] programing language at the University of Maryland, College Park

The volumetric absorption of the solar radiation is rather complicated. Each wavelength has a different rate of absorption and thus heat loads deposited at various points in the CCR are quite different. For this initial discussion, we will consider the sun directly over the CCR, that is, during full moon. Since there does not appear to be a commercial program that handles the volumetric absorption, we have developed such a program based on the IDL programing language at the University of Maryland, College Park.

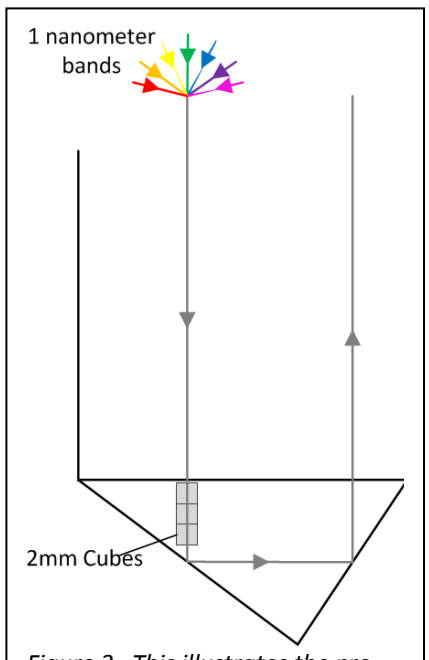

Figure 3 This illustrates the procedure of computing the heat load in each 2 mm cube that a given ray of given wavelength passes through.

Wavelength Dependence:

In order to address the wavelength dependence of the volumetric absorption, the solar spectrum, shown in Figure 1, will be divided into 1 nanometer bands and each of these bands treated separately. In the infrared region, the energy in the solar spectrum drops dramatically thus beyond 5 microns wider wavelength bands are used, in particular, 50 nm steps beyond 5 microns, 1 micron steps beyond 10 microns, and even wider steps beyond 20 microns. The absorption as a function of wavelength can be re-expressed in a manner more relevant to the procedures currently developed by addressing distance that the energy goes in the fused silica before it decreases by 1/e. This is illustrated in Figure 2. Note that this data is for SuperSil 311 produced by the Hereaus Corporation [13 Hereaus], which is a close proxy for the SupraSil 1 used in the Apollo arrays. An input variable allows the choices of other types of glass (SupraSil 1, Clear glass, etc.).

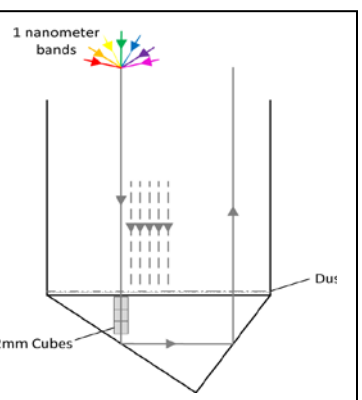

Figure 4 This illustrates the use of many (typically 1000) rays for fully sampling the volumetric absorption in the CCR. It also shows the location of the dust layer.

Thus the treatment of a single ray is illustrated in Figure 3. As the ray enters the CCR in the first 2 mm cube, the absorption or heat load is computed for each 0.1 mm step and the remaining energy remains with the ray as it propagates onward to the next 2 mm cube. Again, the size of the cube used for the calculation is an input variable. As the ray continues, the reflections from the back faces are handled until the ray leaves the CCR, depositing heat loads in each cube along the path.

Multiple Rays:

The above addressed a single ray. This must be repeated for rays spread across the front face of the CCR. At present, we use 1000 rays entering the CCR, distributed in a rectilinear grid over the entire front face of the CCR, as illustrated in Figure 4. Although the number of rays is again an input parameter and can be adjusted, there will be a tradeoff between CPU time and fidelity of simulation.

Dust

Finally, in order to simulate the possibility of dust on the front face of the CCR, we provide a layer that absorbs a specified fraction of the incoming light, and then also absorbs the same percentage of the light as it leaves the CCR. This is gray absorption and provides a heat load that is deposited in the topmost layer of the CCR. This is also illustrated in Figure 4. Based upon the magnitude of the return signal during lunar night, this is estimated at a value of 67% blockage. It's absorption in the visible wavelength range is taken to be 95% and the IR emissivity is taken to be 85%, that is, the values that have been found for the fine particles of the regolith.

Up to this point, the discussion has considered solar illumination that is normal to the front face of the CCR. Of course, the sun will rise, pass through the maximum elevation and then set. For rays that enter the CCR and then leave, thus escaping being blocked by the retaining rings or sun shade, this is a change in the geometry as the ray traverses the CCR. We now define the "aperture" of the system as the opening at the top of the retaining ring, that is, the sides above the CCR. When a ray hits the retaining ring on the way past the aperture, it will deposit a heat load onto the interior of the retaining ring.

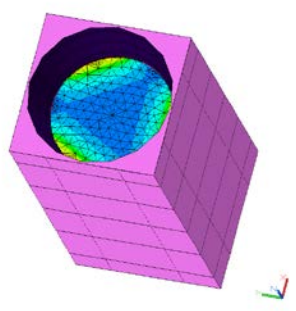

Figure 6 This is an image of the AutoCAD model of the CCR and the housing. The temperature variation of the front face of the CCR is also illustrated.

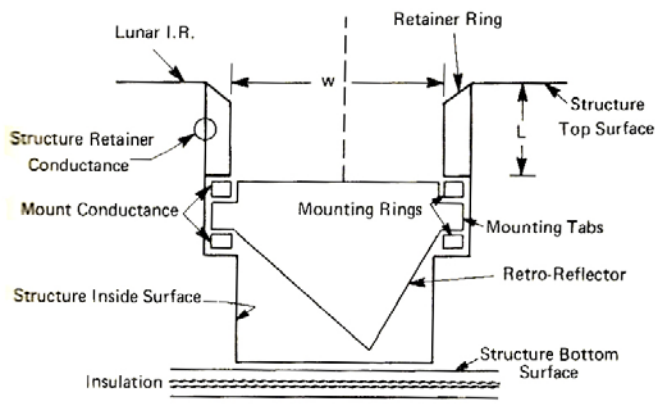

Figure 5 This is a more detailed drawing of a single cell as contained in the panel of the Apollo Retroreflector array, which provides a more detailed description of the AutoCAD model of Apollo CCR and the mounting structure. The entrance aperture (roughly where "w" is shown) is defined at the opening at the lever of the top surface of the structure.

Thermal Modeling

The previous sections address the impact of the solar illumination on the CCR, the retaining ring and the inner surface of the pocket. The IDL program computes the heat load for each of these objects as a function of the motion of the sun during a lunation. We now combine these heat loads with the effect of the sun on the regolith, the exterior of the housing and the internal and external radiation exchanges. This will be accomplished using the commercial package Thermal

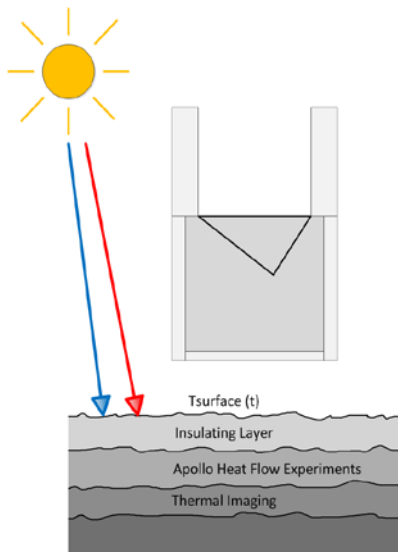

Figure 7 Solar radiation upon the regolith changes during a lunation. These thermal inputs then propagate into the lunar interior.

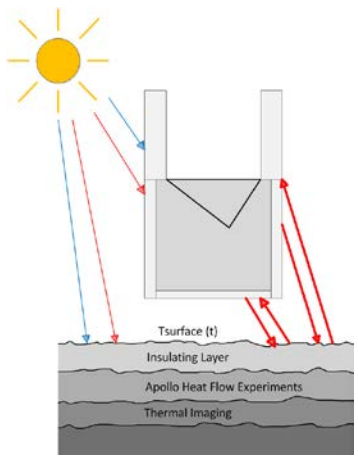

Figure 10 Radiation exchanges between the regolith and the different portions of the exterior of the housing.

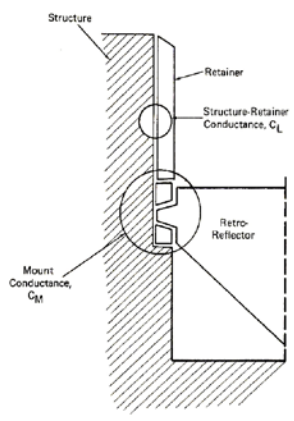

Figure12 Configuration of support of the CCR illustrating the conduction heat paths.

Desktop [14 C&RTech]. The first step is to construct the housing, CCR and retaining ring in AutoCAD. In particular, we must reconstruct the full aspects of the package shown in Figure 5. The AutoCAD model is illustrated in Figure 6. In addition, the orbit of the package about the earth/sun system must be defined in Thermal Desktop, with the ability to switch an eclipse on or off. For the current analysis, this is then suspended 10 cm above the regolith as illustrated in Figure 7. This provides a reasonable simulation of the impact of the support structure on the panel and thus on a single cell.

We initially address the effect of the solar radiation onto the regolith as a function of time in a lunation. Due to the changing properties of the regolith as a function of depth, this model must address the values of conductivity and specific heat as a function of depth. For this reason, we must create a separate model of the regolith in Thermal Desktop in order to determine the temperature of the top surface as a function of time as in input to the housing. The parameters of the various layers are then adjusted so the model fits the data obtained by the Heat Flow Experiment of Apollo 17 [15 Langseth].

The model is shown in Figure 8, which illustrates the temperatures at one instant of time. Thus when the model correctly replicates the data from the Heat Flow Experiment, the temperature of the top surface of the regolith as a function of time is entered as a table into the thermal model for the CCR and housing.

Solar Heating of Exterior of the Housing

Both visible and infrared solar radiation illuminate the exterior of the housing. The angles and thus the apparent absorbing area obviously change as the sun moves across the sky. The heat loads deposited on the exterior depend on the absorptivity in the visible and the absorptivity in the infrared (i.e., (1-emissivity)) as in Figure 9 The initial values of these variables are initially selected based upon the material in the Arthur D. Little Final Report of 1968 [16 ADL], and literature references. They are then fine-tuned based upon the APOLLO observations.

Radiation Exchange between Housing and Regolith

Depending upon the various temperatures at a given time, there are either heat loads on the sides and bottom of the housing or there is energy that is radiated to the regolith. This again depends upon the specification of the infrared emissivity of the sides of the bottom of the housing and the emissivity of the regolith. This is illustrated in Figure 10.

Further Radiation Exchange Heat Loads

In addition to the above, there are a number of additional radiation exchanges. These are illustrated in Figure 11. They consist of radiation from the housing and from the CCR to space, radiation exchange between the retaining ring and the CCR, and between the CCR and the pocket.

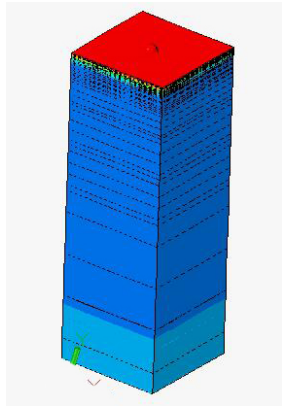

Figure 8 Snapshot of the time evolution of the model of the regolith.

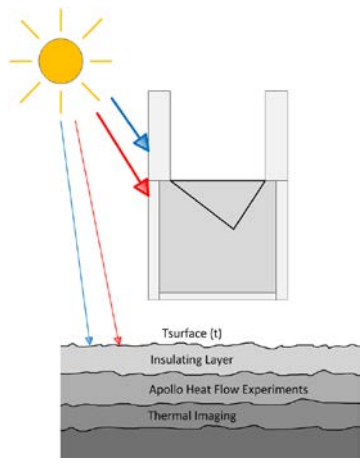

Figure 9 Solar heat loads on the exterior of the housing.

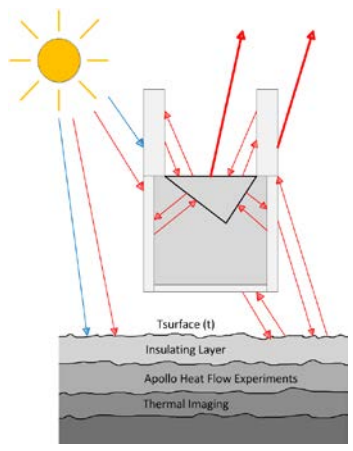

Figure 11 Additional radiation exchanges.

Conduction Heat Loads

Finally, there are conduction heat loads due to the support structure between the CCR and the housing. These are illustrated in Figure 12. This describes the flow of heat through the support rings that contain the CCR within the housing. They are fabricated of KEL-F, a space qualified low conductivity plastic material. There is also a conduction path between the retaining ring and the panel structure that holds all of the CCRs. Again, these values of the conduction are entered as external values for the program. Initially they are chosen to have the values that appear in the ADL Final Report, having been estimated or measured.

Conversion of the Heat Loads to Temperatures

After the computation of the various heat loads, Thermal Desktop takes the above described heat loads and, using the conductivities of the various components of the CCR, the housing and the KEL-F support rings, computes the temperatures of each element in the system as a function of time. These calculations include the recent history, that is, the effect of the finite heat capacity of the various elements. In particular, it determines the temperature of each 2 mm cube, performing this in a time dependent manner in which the array of temperatures of the previous step are used with the new heat loads to compute the next step. The output of Thermal Desktop is then a time history of the temperature of each node. The result is illustrated at one instant in Figure 13.

Temperatures to Optical Performance

The output of Thermal Desktop consists of the temperature of each individual 2 mm cube in the CCR as well as other temperatures of the housing for several hundred time steps spread over a full lunation. We must now convert these temperatures into optical performance. To accomplish this, another series of IDL programs has been created. The index of refraction of fused silica depends upon the temperature and this relation itself depends upon temperature. Thus we may consider a single ray as it enters the CCR. The phase of

radiation associated with this ray has its phase retarded or advanced compared to the mean value of the phase, depending upon the temperature of each of the cells through which it passes. When the ray exits the CCR, the phase delays/advances for a ray that entered the front-face at a given point have built up to some value. We then repeat this operation for each of 1,000 rays. This creates a set of values of the phase delays, or a "phase error map". This process has converted a three dimensional array of temperatures (indices of refraction) to a two dimensional phase error map for each time step during a lunation.

The spatial variation of the phase will cause degradation in the return beam that is going back to the observatory. The return depends on the R.M.S. of the phase error map and this is computed. To determine the signal level at the observatory, a Fourier transform of the phase error map is computed to derive the far-field diffraction pattern, which provides the on-axis signal strength as a function of time during the lunation. However the velocity aberration means that the return will be less than this peak. Thus the return signal strength is also computed for the velocity aberrated observatory, that is, as a function of the latitude of the observatory on earth.

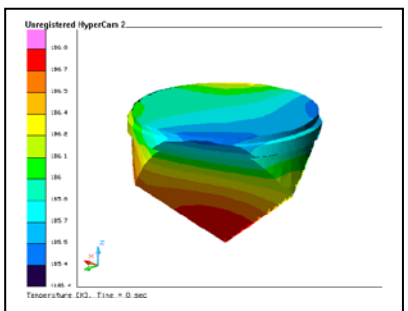

Figure 13 Illustration of the temperature distribution in the CCR. This then reflects the changes in the value of the index of refraction within the CCR.

Code V

When the light reflects from a surface via Total Internal Reflection, there are phase shifts that alter the relation between the input polarizations [17 Chang]. The previous portions of this paper have addressed CCRs that can have a TIR breakthrough on the back face. However, it has not addressed the phase shifts associated with TIR that will occur during a reflection. The current procedure is a more effective approach to study the effect of thermal coatings, sunshade and housing design and other design parameters. However after these have been optimized, one needs to address the effects of the TIR phase shifts and the effects of the offset angles of the back faces that are required in order to correct for the velocity aberration. This auxiliary portion of the simulation is the combination of the LLRRS discussed above with the phase error map derived from Code V with the specification of the offset angles for the back faces combined with the phase offset due to the TIR.

Schematic Representation of Simulation

Up to now, the discussion of the Lunar RetroReflector Simulation (LRRS) has been addressed on a pedagogical format. In Figure 14, this is presented on graphical form.

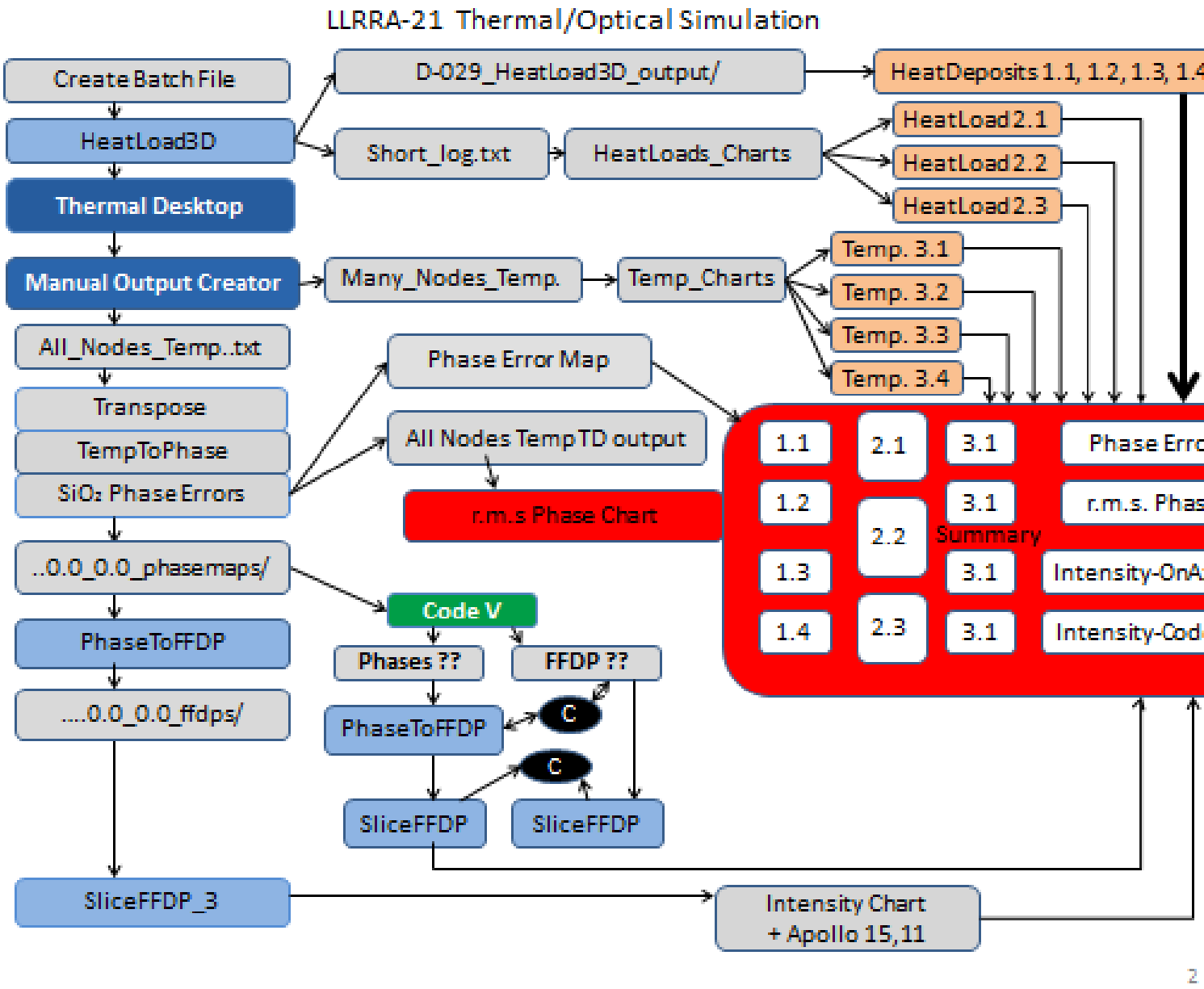

Figure 14 This figure provides a graphic representation of the simulation project. The arrows indicate the flow of the data and/or the commands. The blue elements indicate programs created in IDL and Thermal Desktop. The grey elements are manual inputs or auxiliary files created in the process. The red portion indicates the IDL programs that are used to create the graphical outputs indicated in Figures 16 and 17.

Display of Simulation Results

In order to express these results in a meaningful manner, a summary jpg is created. This contains plots of the more significant results, usually as a function of time during a lunation. In addition, a second jpg is created that addresses the effects in the vicinity of the full moon in order to illustrate the effects during the eclipse. The latter details are critical in the context of the APOLLO observations. The behavior for a full lunation is illustrated in Figure 15. A separate output shows the region around full moon to examine the effects during the eclipse.

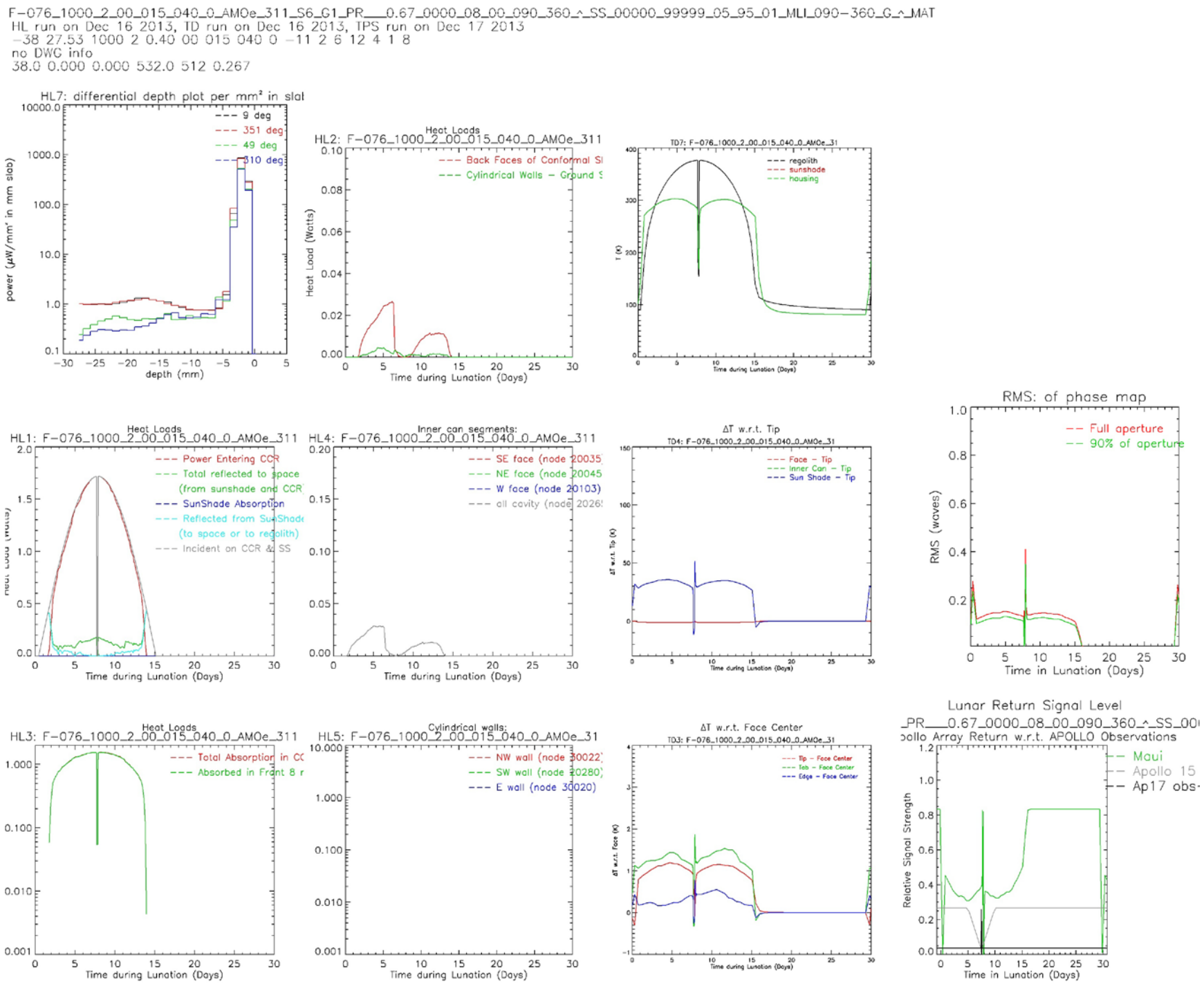

Figure 15 The first two columns illustrate the heat loads that are deposited in the CCR and some of the other elements, as computed by the IDL programs. In particular, the chart at the top left (i.e., location in the first column and first row [1/1]) shows the heat loads within the CCR as a function of depth. Since there is no heat load during the eclipse, this is displayed for the sun off axis by 9 and 45 degrees. The third column describes the temperature distributions as computed by Thermal Desktop. The fourth column addresses the results of the final set of IDL programs that convert the temperature distributions in to optical results, in particular, the R.M.S. of the phase error map and the expected return signal on earth as a function of time during a lunation. This is a case in which a layer of dust on the front face of the CCR is simulated. This is the reason for the very high heat load in the first layer of the CCR as indicated in the upper left figure.

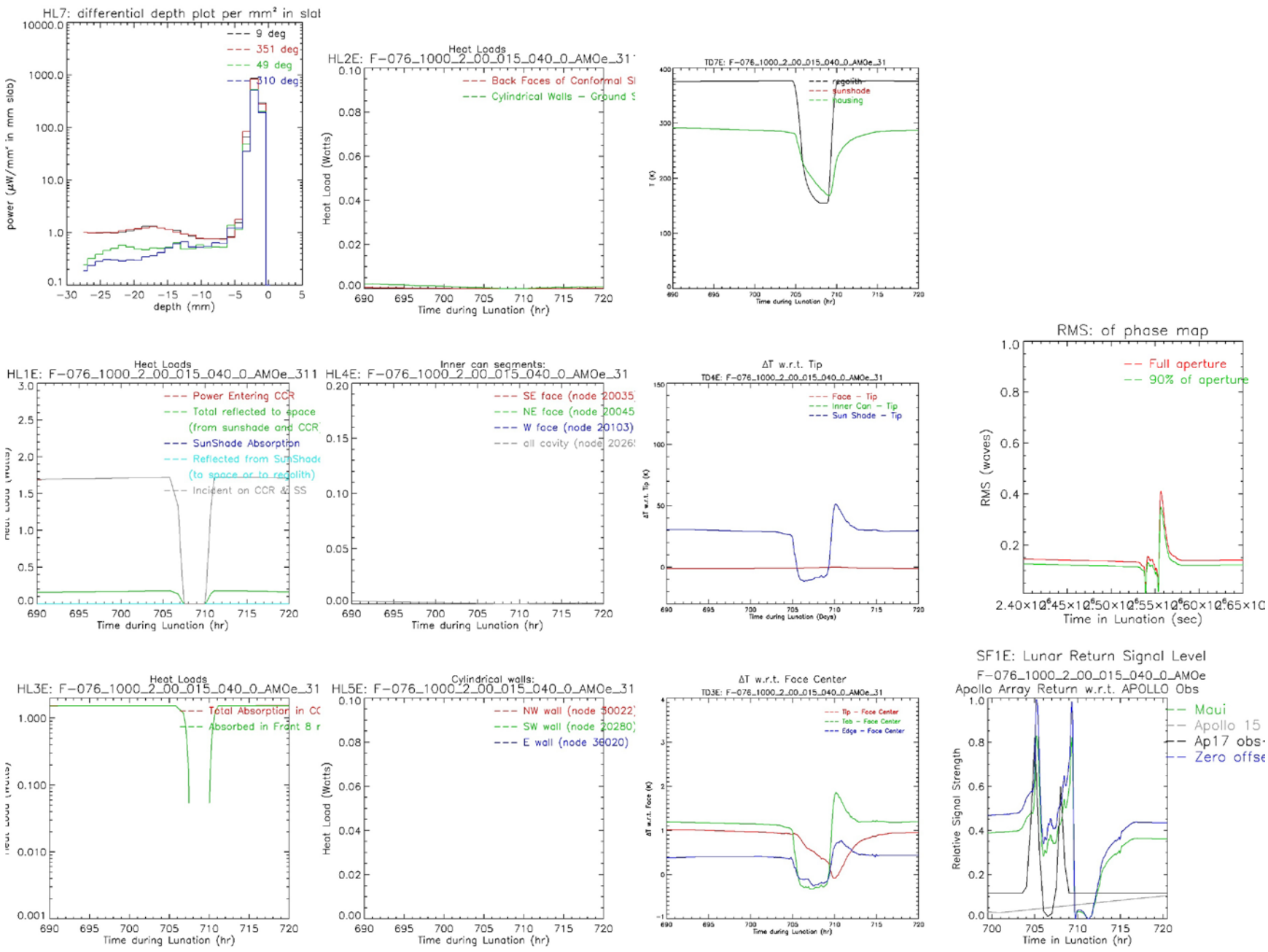

Figure 16 In this case, we examine the behavior in the few hours near the eclipse. In general, the charts are the same as discussed in Figure 15. This allows a detailed investigation of the thermal effects as the radiation of the sun is cut off. The detailed behavior of the solar radiation was provided by Tom Murphy (private communication). Note that the behavior of the return signal shown in the bottom right chart resembles the pair of peaks that were seen in the observations at the APOLLO station during the eclipse.

Conclusions

The investigations to date in operating the lunar laser ranging retroreflector optical thermal analysis program indicates that the LRRS simulation can be a useful tool for optimization of the design of the lunar packages and, in addition, to understand the performance of the Apollo era retroreflector arrays. In a future publication, the results of the application of the LRRS to the detailed observations of the return rates as seen by the APOLLO station will be presented.

Acknowledgements

Portions of this research have been supported by NASA Headquarters via the Lunar Science Sortie Opportunities (LSSO) program, by the Planetary Science Division through the NASA Lunar Science Institute to the University of Colorado under the University of Maryland Contract, as well as support by the University of Maryland, College Park.

Other portions of this research have been supported by the Istituto Nazionale di Fisica Nucleare, Laboratori Nazionali di Frascati (INFN-LNF), Frascati, Italy and the Italian Space Agency (IAS).

DGC would also like to thank John Rzasa for help with the graphics.

References

[1] Currie, Douglas G., Simone Dell'Agnello, Giovanni O. Delle Monache, Bradford Behr and James G. Williams *A Lunar Laser Ranging Retroreflector for the 21st Century* Nuclear Physics B Proceedings Supplements, Volume 243, pp. 218–228 (2013)

[2] Currie, Douglas G., Simone Dell'Agnello and Giovanni O. Monache *A lunar laser ranging retroreflector array for the 21st Century*. Acta Astronaut. V. 68, iss 7-8, p. 667–680 (2011)

[3] Alley, C. O.; Chang, R. F.; Currie, D. G.; Poultney, S. K.; Bender, P. L.; Dicke, R. H.; Wilkinson, D. T.; Faller, J. E.; Kaula, W. M.; MacDonald, G. J. F.; Mulholland, J. D.; Plotkin, H. H.; Carrion, W. and Wampler, E. J. *Laser Ranging Retro-Reflector: Continuing Measurements and Expected Results* Science, Volume 167, Iss. 3918, pp. 458-460 (1970)

[4] Alley, C. O.; Chang, R. F.; Currie, D. G.; Mullendore, J.; Poultney, S. K.; Rayner, J. D.; Silverberg, E. C.; Steggerda, C. A.; Plotkin, H. H.; Williams, W.; Warner, B.; Richardson, H. and Bopp, B. *Apollo 11 Laser Ranging Retro-Reflector: Initial Measurements from the McDonald Observatory* Science, Vol. 167, Iss. 3917, pp. 368-370 (1970)

[5] Bender, P. L.; Currie, D. G.; Dicke, R. H.; Eckhardt, D. H.; Faller, J. E.; Kaula, W. M.; Mulholland, J. D.; Plotkin, H. H.; Poultney, S. K.; Silverberg, E. C.; Wilkinson, D. T.; Williams, J. G. and Alley, C. O. *The Lunar Laser Ranging Experiment* Science, Vol. 182, Iss. 4109, pp. 229-238 (1973)

[6] Williams, J. G.; Boggs, D. H. and Ratcliff, J. T. *Lunar Science from Lunar Laser Ranging* 44th Lunar and Planetary Science Conference, LPI Contribution No. 1719, pp. 2377-8 (2013)

[7] Williams, James G.; Turyshev, Slava G.; Boggs and Dale H. *Lunar laser ranging tests of the equivalence principle* Classical and Quantum Gravity, Vol. 29, Iss. 18, (2012).

[8] Williams, J. G.; Boggs, D. H. and Ratcliff, J. T. *Lunar Fluid Core Moment* 41st Lunar and Planetary Science Conference, LPI Contribution No. 1533, p.2336-7 (2010)

[9] Merkowitz, Stephen M. *Tests of Gravity Using Lunar Laser Ranging* Living Reviews in Relativity, vol. 13, no. 7 (2010)

[10] Murphy, T. W., Jr.; Adelberger, E. G.; Battat, J. B. R.; Hoyle, C. D.; Johnson, N. H.; McMillan, R. J.; Stubbs, C. W.; Swanson, H. E. *APOLLO: millimeter lunar laser ranging* Classical and Quantum Gravity, Volume 29, Issue 18, id. 184005 (2012).

[11] Murphy, T.W., Adelberger, E.G., Battat, J.B.R., Hoyle, C.D., McMillan, R.J., Michelsen, E.L., Samad, R.L., Stubbs, C.W., Swanson, H.E., 2010. *Long-term degradation of optical devices on the Moon. Icarus* 208, 31–35

[12] IDL by Exelis Visual Information Solutions - http://www.exelisvis.com/Company/

[13] Heraeus Quarzglas GmbH & Co. KG - http://heraeus-quarzglas.com

[14] Thermal Desktop by C&R Technologies - http://www.crtech.com/thermaldesktop.html

[15] Langseth, Marcus G., Jr.; Clark, Sydney P., Jr.; Chute, John L., Jr.; Keihm, Stephen J. and Wechsler, Alfred E. *The Apollo 15 Lunar Heat-Flow Measurement* The Moon, Vol. 4, Iss. 3-4, pp. 390-410 (1972)

[16] Arthur D., Little, Inc., *Laser Ranging Retro-Reflector Array for the Early Apollo Scientific Experiments Package.* (1969)

[17] Chang, R. F.; Alley, C. O.; Currie, D. G. and Faller, J. E. *Optical properties of the Apollo laser ranging retro-reflector arrays.* Space Research XII, Vol. 1, pp. 247 – 259 (1972)